EFFECTS OF SKEW ANGLE AND TRANSITION CURVATURE IN HAMR HARD DISK DRIVES

A THESIS SUBMITTED TO THE FACULTY OF
THE UNIVERSITY OF MINNESOTA
BY

MICHAEL CORDLE

IN PARTIAL FULFILLMENT OF THE REQUIREMENTS
FOR THE DEGREE OF MASTER OF SCIENCE

MAY 2017

ACKNOWLEDGEMENTS

First and foremost, I give thanks to God for providing me with the well-being and curiosity to study the infinitely complex world in which we live. My deepest appreciation goes to my parents, Michelle and Jason Cordle, whose love, sacrifice and encouragement have afforded me a life filled with endless opportunities.

I would like to thank the extended HAMR team at Seagate for their continued contributions towards the maturity of HAMR technology, without which my thesis would not have been possible. Although there are too many names to list them all, I would especially like to thank Chris Rea, Tim Rausch, Jason Jury, Josh Christensen, Stephanie Hernandez and Frank Martens, who have supported cross-functional requirements for my research and provided me with many insightful conversations throughout my career at Seagate. I would also like to thank my past and present management teams at Seagate for supporting my pursuit of a graduate degree, namely Ed Gage, Cal Hardie, Preston Sellers, Ed Neu and Dallas Holm.

I would like to extend my gratitude to my committee members, Dr. Randall Victora, Dr. Jian-Ping Wang, and Dr. Anand Tripathi for agreeing to serve on my committee and evaluate my work. I would especially like to thank my adviser, Dr. Randall Victora. It has been my honor to be one of Dr. Victora's graduate students, and his guidance, patience and feedback throughout my graduate school experience cannot be overstated.

DEDICATION

To the memory of my Grandmother Elizabeth “Betty” Manisto (1932–2015)

“*My adventurous, skydiving grandson Michael...He is quite an interesting guy....I love him!*”

Your encouraging words will forever be missed.

ABSTRACT

Continued areal density growth in hard disk drives (HDD) is becoming increasingly difficult to achieve as Perpendicular Magnetic Recording (PMR) approaches the super paramagnetic limit of ~1Tb/in^2. Heat-Assisted Magnetic Recording (HAMR) is on the verge of becoming the next generation of high-density recording technology. Understanding the physical mechanisms behind the unique recording characteristics will be a critical step in the maturity of HAMR technology as it continues to make progress towards production. A notable difference between HAMR and PMR that has drawn a lot of recent attention is the curved shape of a recorded transition. Minimizing transition curvature is understood to be crucial for improving ADC, and current studies have shown that it could be imposing a significant limitation for HAMR. Here, we provide a comparison of HAMR and PMR ADC profiles in an HDD. We explore a new technique proposed for capturing magnetization footprint images through HDD testing, and take full advantage of a significantly improved cycle time to apply a statistical treatment to experimental curvature data to provide a quantitative analysis of factors that impact transition curvature in HAMR and PMR HDDs. We identify geometric effects resulting from skew angle that correlate well to changes in transition curvature. We also show the impact of laser power on transition curvature, and discuss how an understanding of this information can be used to quickly identify uncontrolled variables in an experiment.

TABLE OF CONTENTS

LIST OF FIGURES

Chapter 1 – Introduction to Hard Disk Drives

1.1 Hard Disk Drive Basics

Hard Disk Drives (HDD) are electro-mechanical devices that provide computer systems the ability to randomly store and access non-volatile digital information. HDDs were first introduced to the computing industry in 1956 when IBM announced its 350 Disk Storage Unit, which was a major component of the 305 RAMAC (Random Access Memory Accounting and Control) system. Standing over 5 feet tall with a footprint of 12 ft^2 and weighing nearly 2000 pounds, the 3.75 MB capacity of the IBM 350 was stored on a stack of 50 disks that had a diameter of 24 inches at an areal density of 2k bits per square inch[37]. The advantage of being able to quickly access random pieces of data combined with a consistent exponential growth in areal density has made HDDs the predominant storage device in the computing industry for the past 6 decades.

The success of HDDs has perpetuated through the modern era of computing as a result of an explosive increase in the amount of data being generated. A 2013 study[13] revealed that approximately 2.5 Exabytes (10^{18} bytes) of digital information is generated per day. At that rate, the entire library of digital information in existence just a decade earlier would now be generated over the span of only two days. The rate at which the digital universe is expanding has even out-paced what are already staggering predictions. In 2007, the first annual

white paper on data growth published by the Internet Data Center (IDC) predicted that the global datasphere would reach 988 Exabytes in 2010; however a later study found the actual number to be 1,227 Exabytes[16]. The latest IDC forecast[28] predicts that the world will create and replicate 163 Zettabytes (10^{21} bytes) of data in 2025. As the ability to utilize large sets of data improves, HDDs will likely continue to play a critical role in meeting the global demand for digital storage[11].

Modern HDDs are logical block devices, providing computer systems with a level of abstraction that allows them to more easily manage how data is stored throughout the system. Inside an HDD, data is stored digitally on one or more magnetic disks. The disks are mounted to a spindle motor and rotate at a constant angular velocity. Typically, both the top and bottom surface of the disk are used to store information. To store and access data, a dedicated recording head for each surface is mounted to a mechanical arm, and a stack of one or more arms are attached to a rotary actuator. When an electrical current is applied to the actuator coil, the entire assembly rotates around a single pivot point in order to position the head over a desired location on the disk[12].

The radial position of the recording head is controlled with a high degree of precision and accuracy by a servo controller. Small wedges of information are evenly distributed around the circumference of the disk to provide closed loop feedback of the recording head's current position to the control system. These servo wedges are typically pre-written to the media before the HDD is

assembled. Radial locations on the disk are often described in general terms as existing within one of three ambiguously defined regions of the recording surface that refer to the outer-diameter (OD), mid-diameter (MD) and inner-diameter (ID) of the disk.

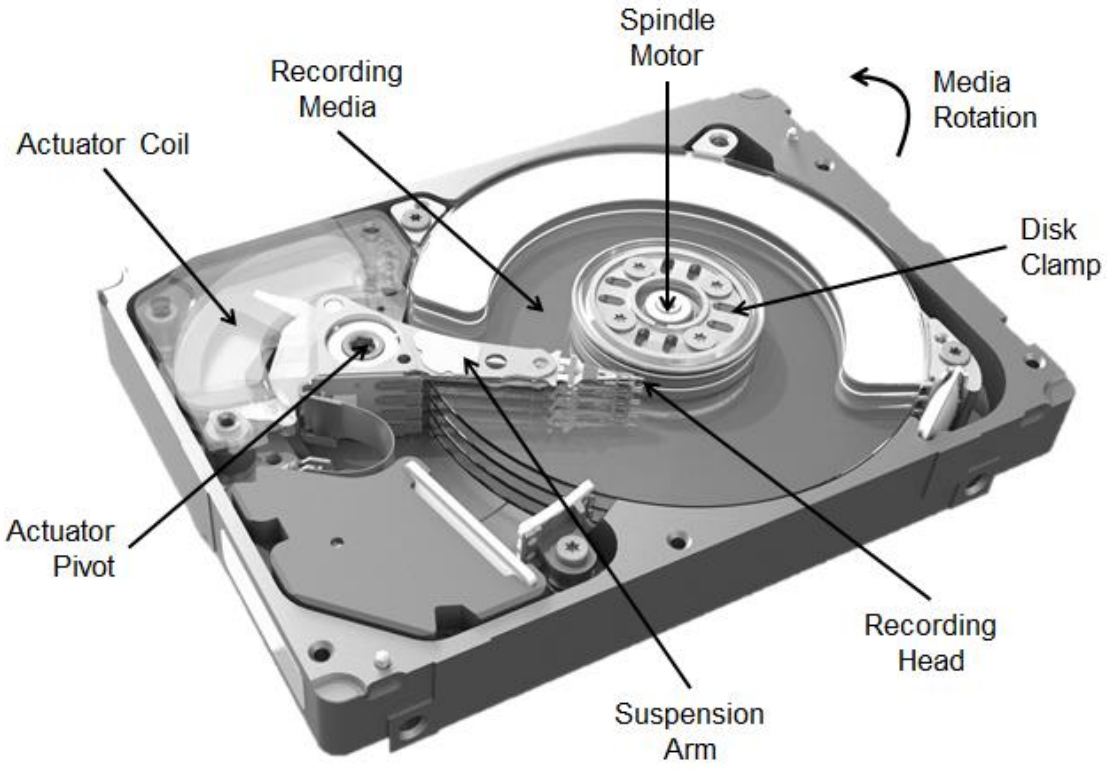

Figure 1.1: Basic components of an HDD

HDDs organize data by dividing each disk surface into tracks and sectors[12]. A track can be described as the circumferential path a head will follow along the recording surface when the actuator is held in a fixed position. A sector is the smallest amount of data that an HDD will write or read from the disk. Each track typically contains multiple data sectors, where each sector consists of either

512 or 4096 bytes of data, plus several additional bytes of information for functions such as addressing, security and error correction. Sectors are also sometimes referred to as blocks, and the two terms are often used interchangeably, however the distinction between them is that a sector describes the information as it physically exists on the media whereas a block describes the information as it is represented in the software that is used throughout the system.

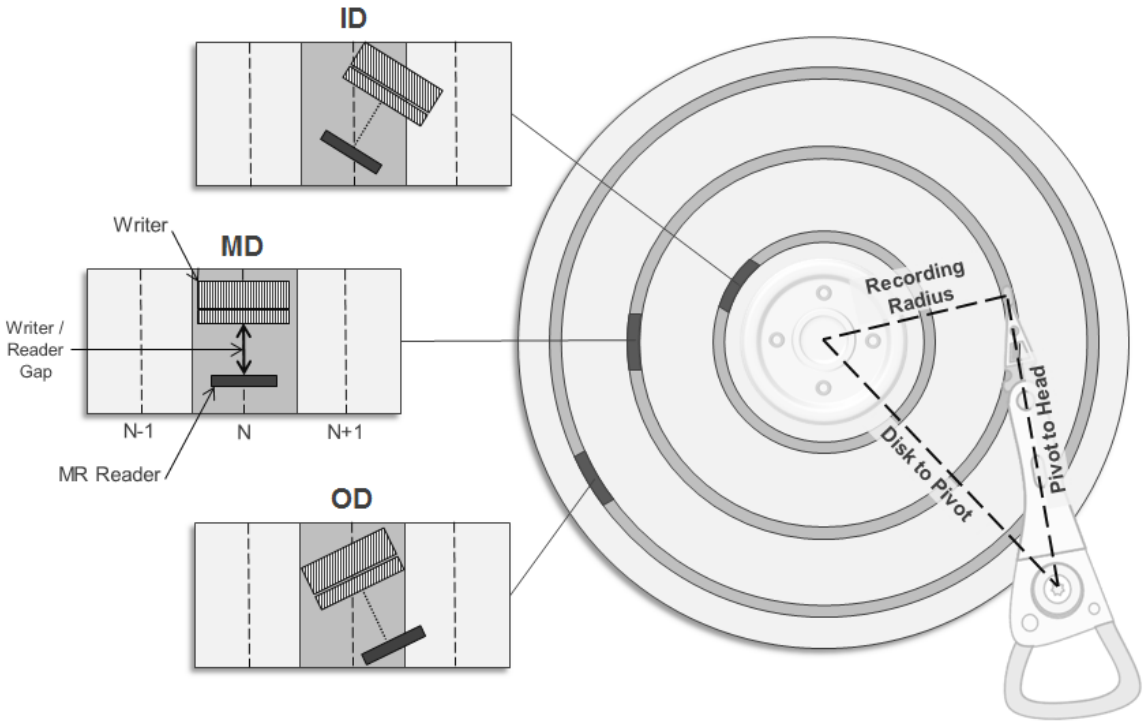

Figure 1.2: Illustration of head skew in an HDD

The tasks of writing information to the media and reproducing that information after it has been written are performed by separate write and read elements designed specifically for their respective purpose. Reproducing data

requires that the reader element is placed as closely as possible to the same position that the writer element was in when the data was written, and the ability to do so accurately will have a direct impact on recording performance. One of the most substantial sources of radially-dependent positioning error between the read and write elements is head skew. Figure 1.2 helps to illustrate to the concept of head skew, where the arc formed by the rotation of the actuator arm around the pivot causes the position of the read and write elements relative to each other and to the concentric track center to change as a function of radial location on the disk.

The skew angle is expressed as the angle that is formed between the centerline that runs through the pivot point and recording head along the length of the actuator arm and a line that is tangential to the concentric track at the location of the recording head[27]. By this definition, when the two lines connecting the recording head to the center of the spindle motor and the recording head to the actuator pivot intersect to form a right angle, the skew angle will be zero. Zero skew is a commonly used reference point when describing head skew as typically the read and write elements will have the best alignment with respect to track center and the effects of head skew are minimized. HDDs are typically designed such that the zero skew position is near the center of the recording area in order to minimize the negative effects of head skew. The magnitude of the skew angle increases as the head moves radially in either direction away

from zero skew and is defined to be positive in the direction towards the OD and negative in the direction towards the ID.

It should be noted that another common use of the term head skew refers to a technique for laying out sectors on the disk in a manner that minimizes rotational latencies during sequential operations that access data stored on more than one track, however the previous definition concerning recording head geometry is assumed throughout this paper.

1.2 Magnetism and Magnetic Recording

Magnetic recording describes the storage of information using a magnetized medium and is the fundamental technology that enables nearly all mid to long term information storage, including HDDs. The magnetic recording media in an HDD is a multi-layer structure consisting of various materials that are deposited sequentially in thin film layers onto a much thicker non-magnetic substrate, with the material and thickness of each layer designed specifically for a unique purpose within the recording system[34]. The storage of information occurs in the recording layer, which is a continuous thin-film layer of ferromagnetic alloy material comprised of many highly ordered crystalline grains. Conceptually, each grain is assumed to be a single magnetic domain, and therefore its magnetization is considered in a saturated state and uniform throughout its volume. The magnetocrystalline anisotropy of each grain describes the property where magnetizing the grain in some directions requires more

energy than it does in others[1]. Since states that minimize the internal energy are preferred, the direction of the grain's magnetization will tend to align to a well-defined symmetry axis that is determined by its lattice structure. The hexagonal materials used in thin-film recording media have a single anisotropy axis and an anisotropy energy that is given by equation 1.1, where K is the anisotropy constant for a given material and θ is the angle between the magnetization and the anisotropy (easy) axis. Equation 1.1 can be used to show that two separate energy minima exist at θ=0° and θ=180°, indicating that the orientation of the magnetization can point in either direction along the anisotropy axis[30].

$$E = K * sin^2(\theta) \tag{1.1}$$

The application of an external magnetic field causes the magnetization to begin to align with the direction of the field. If the effective strength of the applied field is large enough to overcome the anisotropy energy, the magnetization polarity can be flipped from its current low-energy state to the other. The curve in figure 1.3 shows the magnetization (M) response to the strength of an external magnetic field (H) applied along the anisotropy axis, revealing the hysteresis of the material. This hysteretic behavior is the fundamental property that enables magnetic recording.

There are several pieces of useful information that can be extracted from the M-H loop in figure 1.3. The remnant magnetization (M_r), or the magnetization that is retained after the external field has been removed, is found at the points where the curve intersects the vertical axis. The coercivity (H_c), which is the

minimum applied field required to switch the magnetization polarity, occurs where the curve intersects the horizontal axis. The saturation magnetization (M_S) is the maximum magnetization that the material is capable of reaching, which is asymptotically approached as $H \rightarrow \pm\infty$.

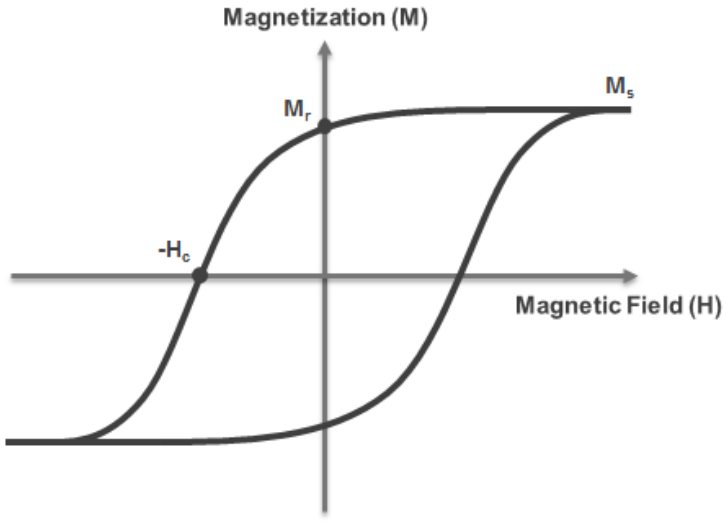

Figure 1.3: M-H hysteresis loop for hard magnetic materials

Information stored on modern HDDs is recorded using a digital format. As the rotating media passes beneath the recording head, the magnetization of the media is averaged over regions containing many grains. Binary values are determined based on whether or not a transition between magnetic states is detected within a synchronous timing window[1]. While there are multiple methods that can be used to store information on continuous thin-film media, the recording scheme most commonly found in modern HDDs is perpendicular magnetic recording (PMR). PMR is named for the orientation of the media magnetization, which points in a direction orthogonal to the surface of the disk.

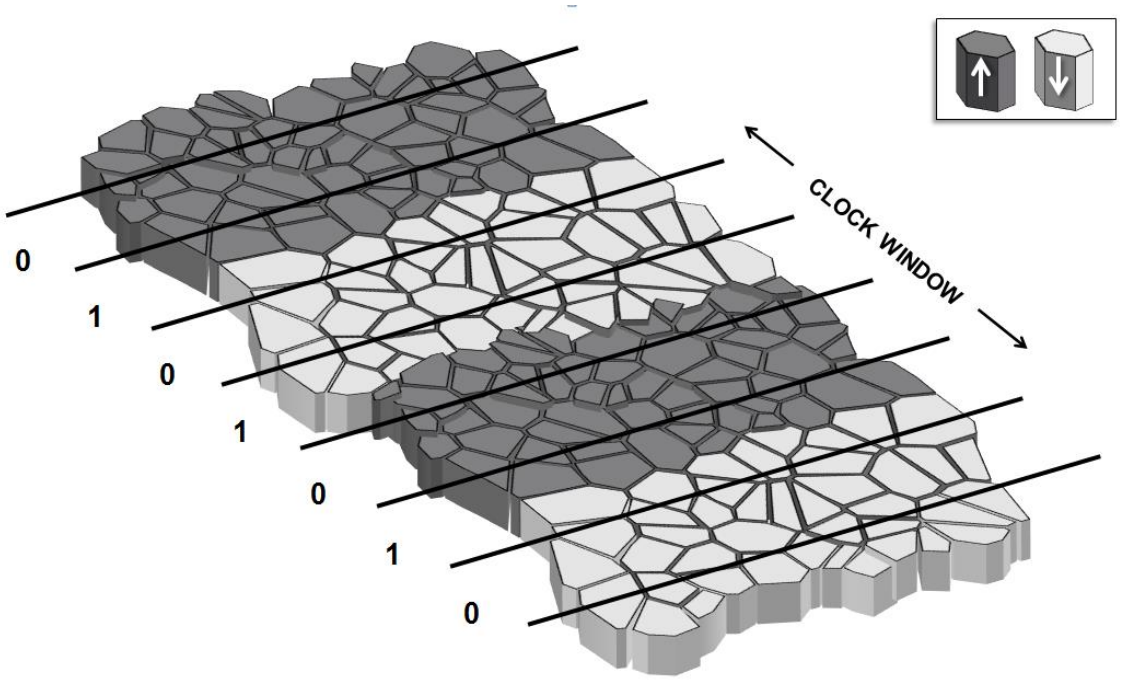

Figure 1.4: Digital magnetic recording

Transitions are written to PMR media using an electromagnetic transducer that consists of a wire coil wound around a highly permeable core. In accordance with Faraday's Law, applying an electrical current to the coil induces a magnetic field in the core, which is then used in close proximity to the media to manipulate patterns its magnetization. The shape of the transducer core is such that it has two poles at the head surface that direct the magnetic flux across the air gap and towards the media. To improve the ability to focus this field to a localized area of the recording surface, PMR media includes a layer of magnetically soft material called the soft under-layer (SUL) that is deposited below the recording layer[34]. The induced magnetic flux passes from the transducer core through the recording layer and into the SUL and then back through the return pole. The high

permeability of the SUL allows us to assume that the entire core structure is magnetically “imaged” in the SUL, further increasing the effective field. The return pole of the transducer is designed to have a much wider surface area than the main write pole, effectively decreasing the field density of the return path in order to avoid unintentional down-track erasure[34].

The information stored in the magnetization pattern written to the media is later reproduced using a magnetoresistive (MR) sensor to detect changes in the magnetic flux on the media. The electrical resistance of an MR sensor is highly sensitive to external fields due to the magnetoresistive effect, where spin polarized electrical current flows more easily though a magnetized material when its magnetization is aligned in parallel to the spin orientation of the majority charge carrier as opposed to when the alignment of the magnetization is anti-parallel[1]. A bias current is applied to the MR reader so that it operates in its highest region of sensitivity, in which case the voltage measured across the device closely resembles the electrical current signal that was supplied to the transducer when the pattern was written. Predicting the voltage response of the MR reader requires accounting for the dynamic interaction between the media flux and the magnetic properties of the recording head. This interaction is more easily understood using the reciprocity principle[1], which uses a mutual induction approach to evaluate the system as a whole.

Chapter 2 – Areal Density Capability

2.1 Formalism of Areal Density Capability

Areal density describes the amount of information stored on the media per unit of surface area, and has maintained an exponential compound annual growth rate (CAGR) since HDDs were first introduced in 1956. To put this in perspective, if the 2 Kbit/in^2 areal density of the original IBM 350 were adjusted to the ~1 Tb/in^2 of today's HDDs, neglecting any other improvements in format efficiency, it would offer a total storage capacity of 1,875 TB. In the time from 2003 to 2013, the average capacity of an HDD had increased from 17 GB to 565 GB while the number of units shipped annually made a more modest increase from 200M to 600M[14]. This indicates that the increase in total storage capacity is dominated by increases in areal density, which means the surface area of each recorded bit is getting smaller.

Areal Density Capability (ADC) is a key metric for gauging growth in magnetic recording technology and directly impacts critical metrics at the system level such as capacity, performance and reliability[11]. The smallest size to which a recorded bit can shrink is ultimately limited by the maximum achievable signal-to-noise ratio (SNR) of the recording system. The noise present in an HDD can be categorized into three sources: media noise, head noise, and electronics noise. Modern HDDs are considered to be media noise limited since it is the dominating

contributor across nearly the entire frequency spectrum[2, 35]. The media SNR is proportional to the number of magnetic grains per recorded bit. Increasing areal density while maintaining SNR requires fitting the same number of grains within a smaller surface area, meaning the size of each grain needs to become smaller.

The challenge with reducing grain size is maintaining thermal stability. The probability of the grain's magnetization polarity randomly changing state due to thermal fluctuations over time is governed by the superparamagnetic limit[30] given in equation 2.1, where f_o is the attempt frequency, K_u is the anisotropy energy, V is the grain volume, K_B is the Boltzmann constant and T is the temperature. We can see from the two terms in the numerator of the exponent in this equation that maintaining thermal stability in smaller magnetic grains requires using magnetic alloys with a proportionately higher anisotropy.

$$\tau = \frac{1}{f_o} * \exp\left(\frac{K_u * V}{K_B * T}\right) \tag{2.1}$$

Moving to higher anisotropy translates directly into higher coercivity, meaning the external field strength produced by the transducer must increase accordingly in order to maintain the ability to write the media. Unfortunately, recording heads are subject to another fundamental limitation[3]. For the known magnetic materials that are able to be used recording heads, the Slater-Pauling curve places an upper bound on the magnetic flux density in the transducer core at approximately 2.4 T. This three-way interdependency between SNR, thermal stability and media writabillity is known as the magnetic recording "trilemma".

2.2 Heat Assisted Magnetic Recording (HAMR)

Applying the superparamagnetic limit to PMR finds the upper limit of the maximum achievable areal density to occur at approximately 1 Tb/in^2, and the latest generations of HDD products are quickly approaching this limit. Extending areal density beyond this limit will require a new approach, and currently the most feasible successor to PMR is Heat Assisted Magnetic Recording (HAMR).

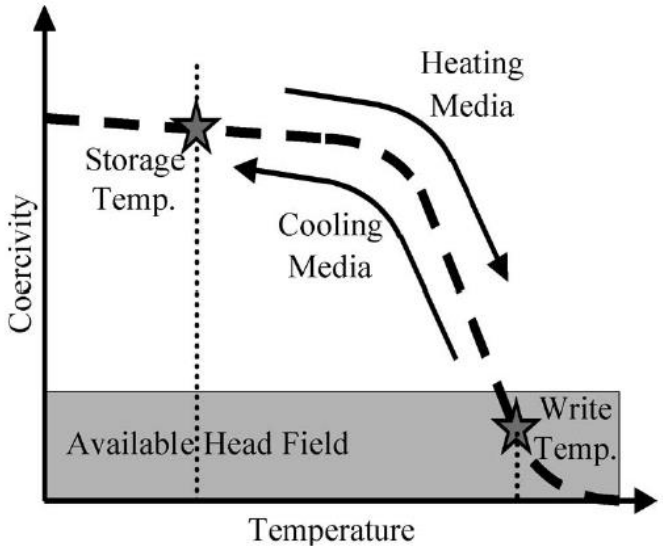

Figure 2.1: HAMR write process

As its name suggests, HAMR addresses the superparamagnetic limit through temperature by temporarily heating a localized area of the media as the magnetic pattern is written. In most embodiments of HAMR, the media is heated using an integrated optical system consisting of a laser diode, a near-field transducer (NFT), and a coupling mechanism[14]. HAMR relies heavily on the

dependence of coercivity on temperature, particularly near the Curie temperature (T_c), which specifies a critical temperature above which the anisotropy and magnetization of the media become negligible[1]. Applying power to the laser creates a tightly focused optical spot directly beneath the recording head that heats the media above T_c before rotating out of the thermal spot and passing under the magnetic write pole. As the media quickly cools to ambient temperature in the presence of an applied magnetic field, the anisotropy is restored to a nominal value and the magnetization remains aligned with the field direction[3].

$$\frac{\partial H_{eff}}{\partial x} = \frac{\partial H_w}{\partial x} + \frac{\partial H_K}{\partial T} * \frac{\partial T}{\partial x} \tag{2.2}$$

The quality and characteristics of a written transition are determined by the effective switching field gradient. In the case of HAMR, the switching field gradient is given by equation 2.2, where the effective gradient is a combination of the field produced by the writer (H_w), the slope of the anisotropy field (H_k) as a function of temperature (T) and the spatial variation of the thermal profile in the media. The relationship between H_k and T is an intrinsic property of the recording medium and H_w is often assumed to be spatially uniform, therefore the effective gradient of a HAMR storage system is considered to be dominated by the gradient of the thermal profile. Effective write field gradients can be achieved in HAMR that are easily an order of magnitude larger than field gradients found in conventional PMR[3].

Modern HDDs store information at track widths below the diffraction limit of visible light[3]. Since the write process is dominated by the thermal profile, achieving ADC growth with HAMR requires the ability to focus light to spot sizes well below the diffraction limit. The NFT is a critical innovation that utilizes surface plasmon resonance to make HAMR technology feasible by modern standards. This is possible because surface plasmons are an electromagnetic mode that couple the electrons to the free space fields and therefore have an effective wavelength shorter than the light that excites it[36]. This enables HAMR to simultaneously achieve higher effective field gradients and higher track densities compared to PMR, providing an exciting opportunity for continued areal density growth in the near future.

2.3 Comparing HDD Recording Schemes

The areal density in HDDs is typically reported in bits per square inch and is easily calculated by multiplying the number of media flux changes (or bits) per inch in the circumferential direction by the number of tracks per inch in the radial direction[11]. The ratio of bits per inch (BPI) to tracks per inch (TPI) is called the aspect ratio, which describes the width to length ratio of a recorded bit.

Although ADC is an incredibly meaningful metric in magnetic recording, using it to compare one design or technology to another can sometimes be difficult because the criterion for what makes a recording system “capable” is often subjective. To address this problem, a method was recently proposed[7] as

an industry-wide standard for experimentally measuring and comparing ADC. As it applies to conventional (non-shingled) versions of PMR and HAMR, this method requires that first a test track is written to the media, and then the adjacent tracks on both sides of the test track are written 32 times each. The adjacent tracks are written using different encoded random data patterns under the same recording conditions as the test track. The written data must include a minimum of 50 data sectors that are 4 kB in length, which are re-read from the test track without applying any additional error correction until 10,000 consecutive sectors have been read. The highest areal density where this procedure can be performed without any erroneous sectors is determined to be the areal density capability.

To demonstrate how the sensitivity of ADC to recording position in an HDD is significantly different between PMR and HAMR, this procedure was performed at various locations distributed across the entire recording surface for groups comprised of 10's of HAMR and PMR drives. ADC was measured across a full range of BPI and TPI settings, and in the case of HAMR, laser power was also allowed to vary. All other parameters were held constant at nominal conditions which are typical of field operation. Figure 2.2 shows the measured ADC normalized to the maximum value of each surface as a function of disk radius for HAMR and PMR. To illustrate the profile shape across the stroke, the piecewise interpolated average for each group is shown using a solid line for HAMR and a dashed line for PMR. This data shows that for PMR HDDs, the

maximum ADC is achieved at a location near the MD, and appears to roll off symmetrically as the head moves to either side of this point. On the other hand, the ADC profile in a HAMR drive is asymmetrical across the stroke and heavily favors the ID of the disk.

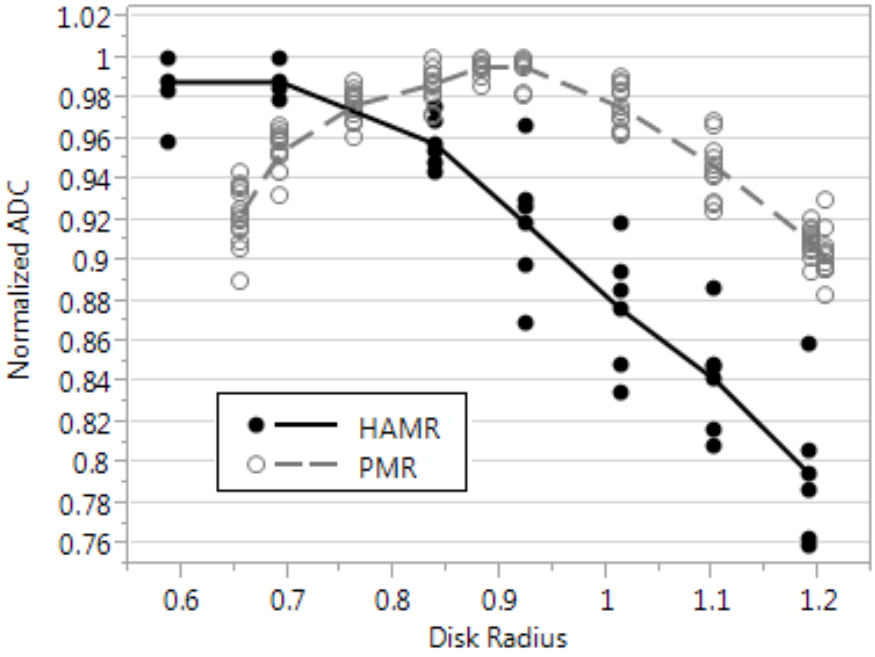

Figure 2.2: ADC profile comparison between HAMR and PMR

Understanding the physical mechanisms that drive these profiles to appear so fundamentally different will be a critical step towards the maturity of HAMR technology. A notable difference between HAMR and PMR that has drawn a lot of recent attention is the curved shape of a recorded transition. Minimizing transition curvature is understood to be crucial to improving ADC, and the following chapters are dedicated to experimental studies that explore several aspects of transition curvature in detail.

Chapter 3 – Transition Curvature

3.1 Characterizing Transitions

In an ideal recording system, a written transition from one magnetization polarity to the other will occur instantaneously at a fixed location in the down-track direction (x) independent of cross-track position (z). In practice, the transition occurs over some non-zero distance in the down-track direction due to the imperfect alignment of the grains on either side of the transition. The magnetization distribution across a transition is described by equation 3.1 where *x* is taken in the down-track direction, M_r is the remnant magnetization, and *a* is a constant proportional to the transition width that is commonly referred to as the transition parameter[1].

$$M(x) = \frac{2M_r}{\pi} tan^{-1}(x/a) \tag{3.1}$$

Magnetic transitions in high-density recording also exhibit a curved shape in the cross-track direction. As shown in figure 3.3, curvature has a significant impact on off-track read performance[23, 25] by introducing a phase delay in the read-back signal. Transition curvature has been shown to play an important role in on-track performance loss as well[10, 18]. Early recording models accounted for curvature as variation in transition width, which is also how it is typically observed experimentally. However, unlike transition width, the spectral response of amplitude loss to transition curvature at high frequencies is non-linear and

therefore must be considered as a separate effect[10]. Transition curvature is an important characteristic to consider when examining areal density capability because unlike many other factors that limit the recording system, curvature affects both on-track and off-track performance[8, 18]. The off-track performance determines track pitch capability and on-track performance determines linear density capability.

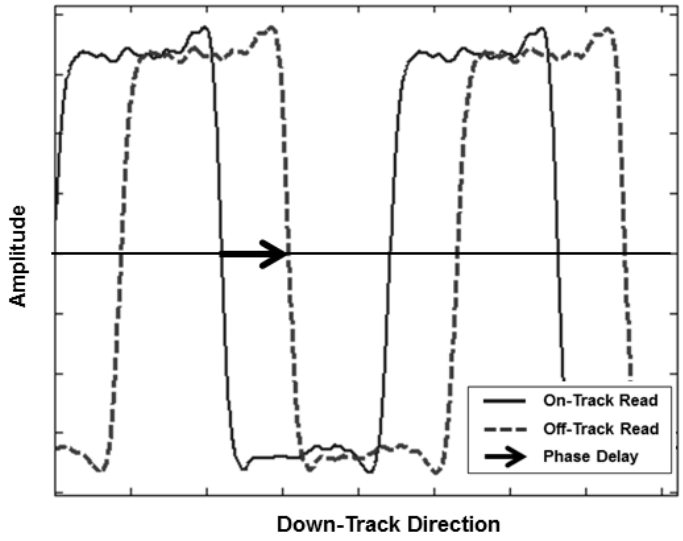

Figure 3.1: Read-back signal phase shift due to reader offset position

3.2 Microtrack-Based Magnetic Footprinting

The most direct methods of measuring curvature once a pattern has been written involve removing a disk from the spinstand or drive and using metrologies such as magnetic force microscope (MFM) to physically examine the magnetization pattern[10, 18]. Despite providing a high degree of accuracy, this type

of analysis can be time-consuming and destructive, and therefore is not practical for large-scale experiments[20].

Footprinting is an increasingly popular tool used to recover an image of the magnetization pattern on the media using the voltage response of the MR reader. This type of analysis has been demonstrated to provide similar results to MFM images and allows for the same head/media combination to be tested under various recording conditions[21]. Footprinting is performed by capturing the voltage wave form from the reader at closely-spaced reader offset positions in the cross-track direction. The resulting series of waveforms are overlaid onto a single plot with one axis representing their respective offset position creating a two-dimensional scan-line image of the magnetization pattern of the media.

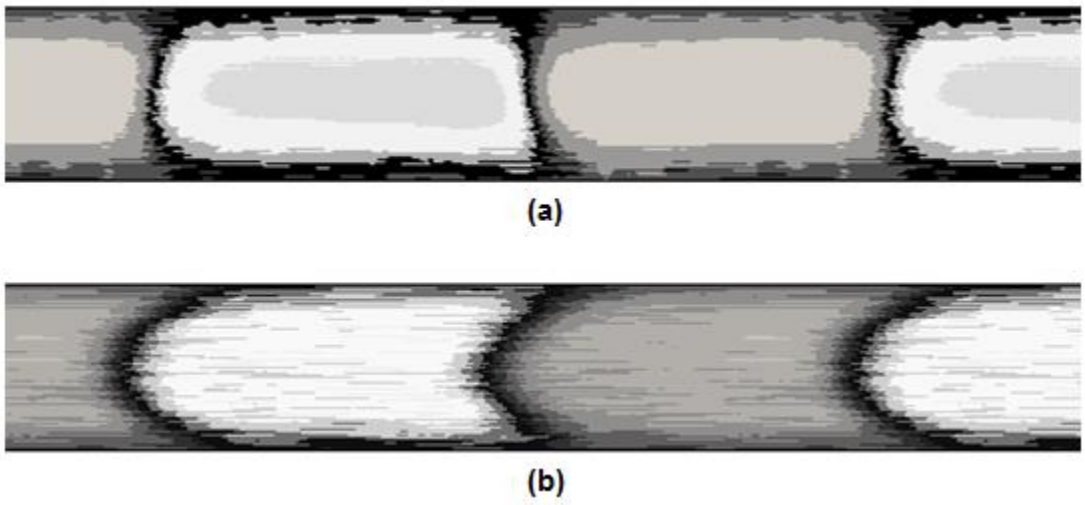

Figure 3.2: Impact of reader width convolution on magnetic footprint

Previous studies[20, 21] have shown that achieving an accurate reconstruction of the written pattern in this manner can be challenging. The voltage signal output by the reader is heavily distorted by the convolution of the reader sensitivity function with the media magnetization pattern due to the finite cross-track width of the read element. In addition, the significantly large reader width causes a cross-track averaging effect which typically results in measurements that under-estimate recording parameters such as transition curvature[20]. Early methods to account for finite reader width effects required measuring the reader response to bulk-erased AC noise in order to deconvolve the reader reciprocity from the written pattern, but this approach has also been shown to have significant potential for providing inaccurate results.

The most effective method known to mitigate the negative influence of reader width effects is through an approach that uses some form of microtrack-based measurements. A microtrack is an isolated section of a written track that is created by trimming the track using AC-erase writes adjacent to each side of the track. In doing so, only a fraction of the original pattern is focused to a narrow portion of the reader width, effectively simulating the conditions of a localized, narrow reader. To produce an image that encompasses the full width of the written track, multiple trimmed microtracks are created at tightly-spaced offset positions distributed evenly in the cross-track direction[9]. After a center-aligned signal trace has been acquired for each microtrack, the signals are phased-aligned based on a cross-correlation of the AC background noise, and then

combined to create a 2D image of the magnetization footprint. This has been the preferred method of microtrack-based imaging for several years[4,8,9]. Even though this is a major improvement over using MFM and various reader deconvolution techniques, it is not without its own limitations. The iterative nature of writing, trimming and reading the required number of offset microtracks still takes a significant amount of time to produce a single image, and the need to re-align the phase of each offset trace presents several possible sources of substantial measurement error[5].

3.2.1 Transverse Microtrack Method

A new approach to footprinting has recently been introduced[5] that eloquently addresses the limitations of previous discrete-microtrack based methods. In this approach, the same principle of using a microtrack to remove the reader averaging effect is used. However, instead of dividing the data track into discrete sections, a single, continuous microtrack is created by trimming the microtrack at a slight angle to the axis along which it was written.

Schematic diagrams outlining the procedure of transverse microtrack footprinting are provided in figure 3.3. In this method, a low frequency single tone sample pattern is written within one wedge-to-wedge timing window. Before any trimming occurs, an on-track reference trace is acquired to determine the period of the written pattern, which is illustrated by the dashed lines in figure 3.3 (a). A sinusoidal signal is introduced into the servo positioning system that causes the

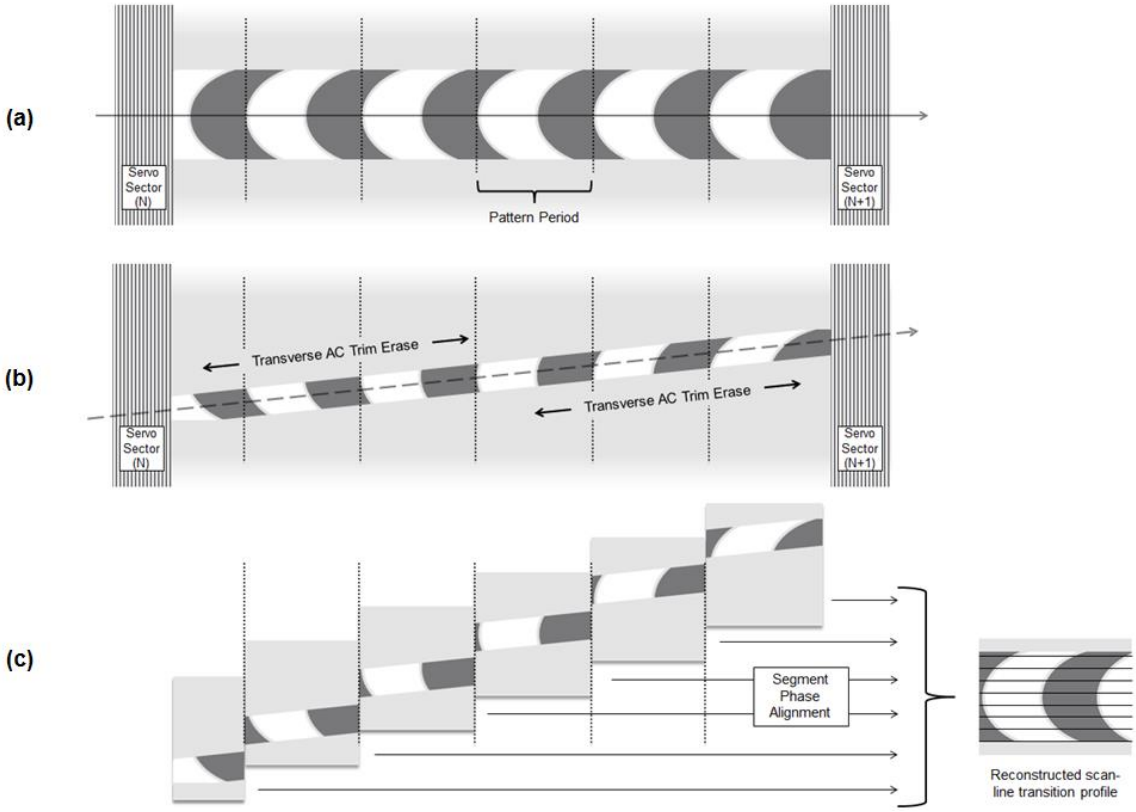

Figure 3.3: Transverse microtrack footprinting method

head to slew across the previously written data along a transverse trajectory. As shown in figure 3.3 (b), offset erases are performed to trim the transverse microtrack along this trajectory, and then a signal trace is acquired along the center of the transverse microtrack. The transverse signal trace is then divided into segments, where each segment represents a slightly different cross-track offset position. The length of each segment is a positive integer multiple of the signal period that was determined from the concentric reference trace. The final step is shown in figure 3.3 (c), where the individual segments are combined to

create a 2D scan-line image containing several cycles of the sample pattern magnetization. The resulting image is similar to the footprint image obtained using an iterative discrete-microtrack approach, but with significantly improved cross-track resolution and can be acquired in a fraction of the time.

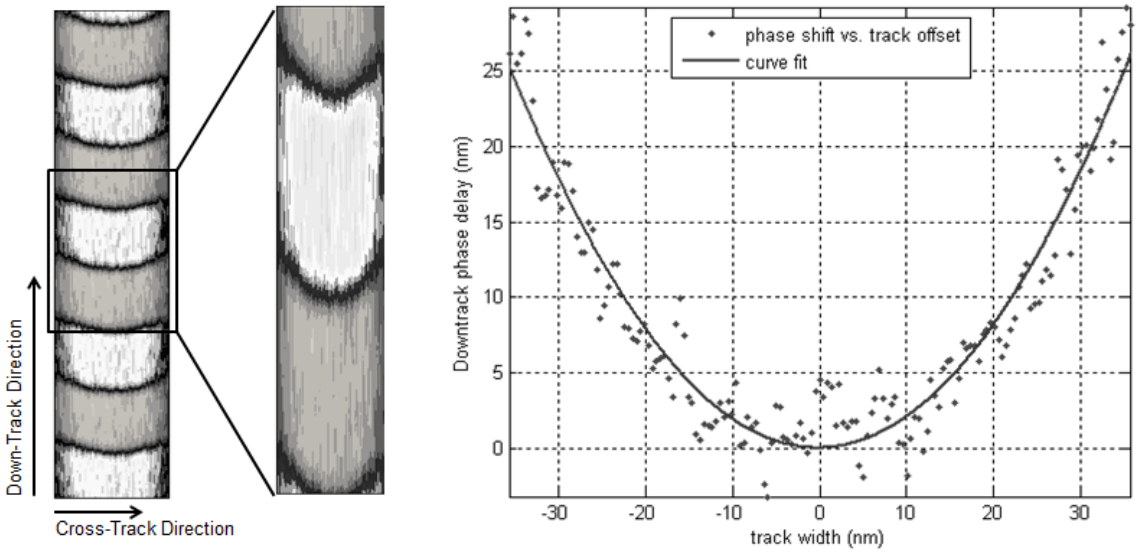

Figure 3.4: Extracting transition curvature from footprint image

Processing the signal traces can provide parametric results of recording characteristics such as transition curvature that can be used for quantitative analysis and comparison[5]. An average cross-track curvature profile is determined by first finding the down-track phase shift with respect to the reference trace for each of the segments used to create the 2D footprint image. The phase shift and its corresponding cross-track offset form a single data point for each transverse trace segment. A curvature profile is determined using a least squares approach

to fit a quadratic polynomial to this data set, as shown by the example in figure 3.4, where the cross-track position is assumed to be an independent variable.

3.2.2 Experimental Setup

In the following sections, the transverse microtrack footprinting method is used to measure and compare written transition curvature in an HDD. Unless specified otherwise, all HDD measurements occur with the disks spinning at 10.5k RPM in a 2.5-inch form factor. Read-back voltage signals are captured using a digital oscilloscope. Drives are tested in an environment that minimizes disturbance from external mechanical vibrations. HDD case temperature is consistent at approximately 1-2°C above ambient room temperature, and held within +/- 1°C for all measurements included in a given experiment. The clearance between the head and media surfaces is actively controlled to maintain a constant spacing between that is consistent with typical drive use. The laser power in HAMR drives is chosen by finding the best error rate in the presence of adjacent track writes in a similar manner used in previous HAMR HDD studies[6]. The bit length and servo-defined track pitch used are approximately equivalent at all locations on the recording surface.

Our measurement technique deviates slightly from the original description of the transverse microtrack method given in section 3.2.1 in that the roles of the concentric and transverse track trajectories have been swapped so that the sample pattern is written along the transverse track trajectory and trimmed along

the concentric track trajectory in order to more accurately control the offset position of the writer during trim writes. Transverse microtracks are trimmed to widths of 25% to 30% of the full track width and the edges of the re-constructed track profile are defined on either side at the cross-track offset where the average signal amplitude has dropped below 50% of the on-track value. The length of the reconstructed footprint image is chosen to include 4 full cycles of the sample pattern.

Many previous studies[9,10,15,18,21-23] have introduced their own various metrics for quantifying transition curvature. Leveraging from this work, the experimental results in the following sections are quantified in two different ways. The first is simply by using the second-order coefficient c from the quadratic fit $cz^2 + bz + a$ in units of nm^{-1}. The second metric used is the maximum deviation in the location of the transition along the down-track direction. In terms of how this applies to the curvature profile, we are taking the down-track distance from the nose to the furthest tail at the edge of the track. Determining which metric is most suitable depends whether we are interested in on-track or off-track performance. Since our goal is to improve the general understanding of transition curvature, both values will be included in our results. Sample size selection is covered in detail in the next section. Unless specified otherwise, all experimental results in this paper are found by taking the average of 10 repeated measurement samples in order to improve uncertainty.

3.2.3 Measurement Capability Analysis

To properly quantify transition curvature using the transverse microtrack method, we will first evaluate the measurement capability of this experimental setup. In this section we apply a statistical treatment to a reasonably large number of repeated measurements as well as provide a quantitative comparison to results from previous experiments in order to establish the accuracy and repeatability of our measurement system.

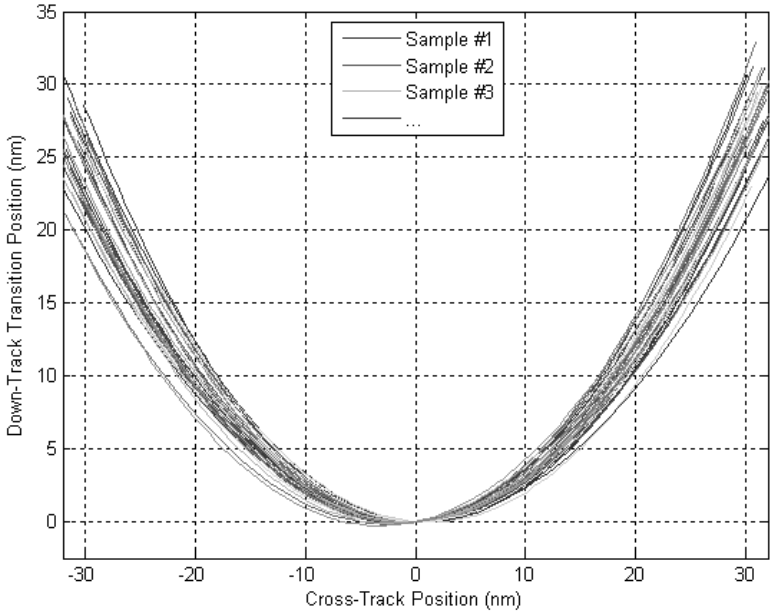

Figure 3.5: Variation of repeated curvature profile measurements

Figure 3.5 shows the fitted curvature profiles from 40 individual measurements repeated within the shortest possible time span using the same experimental setup to test the same drive at the same disk location under the same recording conditions for each measurement.

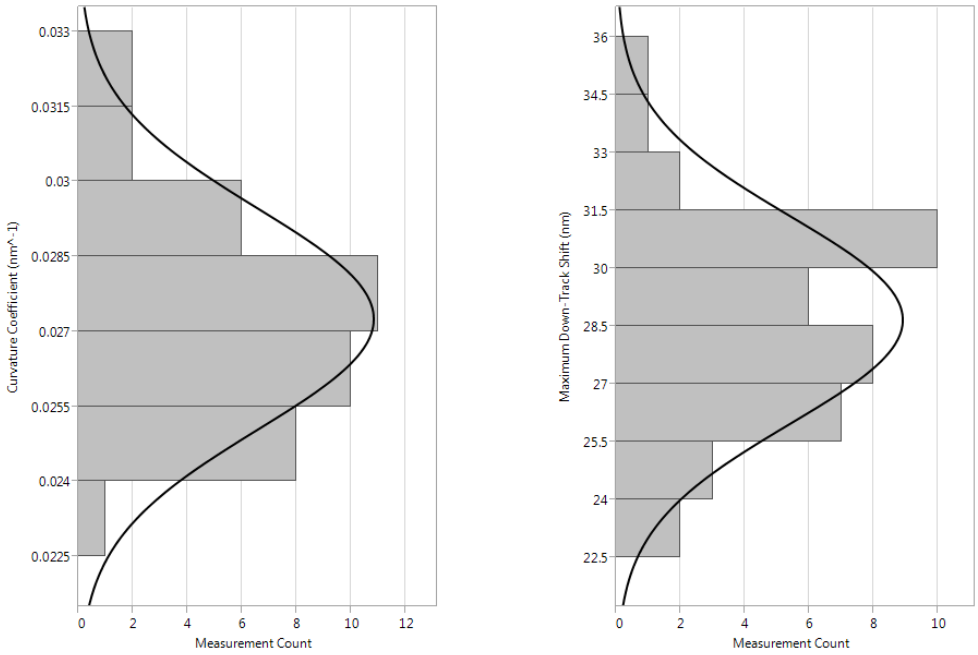

Figure 3.6: Distributions of curvature coefficient and down-track phase delay

Distributions of the curvature coefficient and maximum down-track phase shift are shown in figure 3.6 and include a dark line to show the continuous curve fit of a normal (Gaussian) distribution. A Shapiro-Wilk test is used to determine the goodness of fit to a normal distribution, yielding p-values of 0.73 and 0.627 for the coefficient and phase shift distributions respectively, indicating that the assumption of normally distributed variation in both metrics is very reasonable.

$$\Delta(a,b)|_{min} = \sqrt{\frac{4\sigma^2(Z_{\alpha/2} + Z_{\beta})^2}{N}} \tag{3.2}$$

The mean value of the curvature coefficient is 0.027 nm^{-1} with a standard deviation of 0.0022 nm^{-1}. The down-track phase delay has a mean value of 28.6 nm with a standard deviation of 2.69 nm. With this information we can calculate

our measurement uncertainty at a 95% confidence interval when the mean of 10 measurement samples is used. We find the measurement uncertainty to be 0.00137 nm^{-1} and 1.67 nm for the coefficient and down-track delay metrics respectively.

The minimum detectable difference ($\Delta|_{min}$) between the mean values of two groups of measurement samples a and b that contain a combined total of N measurements can be determined using equation 3.2, where σ is the (assumed) standard deviation, and the variables $Z_{\alpha/2}$ and Z_{β} are coefficients of a normal distribution determined by the statistical power and confidence interval desired for a given experiment. A 95% confidence interval and 80% statistical power are common values chosen to provide a reasonable level of statistical certainty[33], and correspond to coefficient values of $Z_{\alpha/2} = 1.96$ and $Z_{\beta} = 0.84$. Applying the standard deviations from our repeatability experiment, and again choosing a sample size of N = 20 total measurements (N/2 = 10 measurements in each group), we find that the minimum detectable difference in the curvature coefficient is 0.0029 nm^{-1} and similarly for the down-track phase delay is 3.57 nm. This corresponds to detectable differences of 10.75% and 12.45% with respect to the means of the distributions in figure 3.6.

To improve confidence in our results and identify any potential measurement bias or systematic errors, we leverage modeled and spinstand curvature data from another recent study[4] to provide a benchmark for comparison. Three HAMR curvature profiles are shown in figure 3.7 that were

obtained by applying distinctly different methods to a similar head and media configuration. The modeled profile was derived from the magnetization patterns generated by a Landau-Lifshitz-Gilbert (LLG) based simulation, with a curvature coefficient of 0.0182 nm^{-1} and maximum down-track offset of 37.1 nm. The profile measured on spinstand was found using a discrete-based microtrack method and has a curvature coefficient of 0.0141 nm^{-1} and maximum down-track offset of 37.1 nm. The HDD profile was measured using the experimental setup described in the previous section and resulted in a curvature coefficient of 0.0131 nm^{-1} and a maximum down-track offset of 15.9 nm.

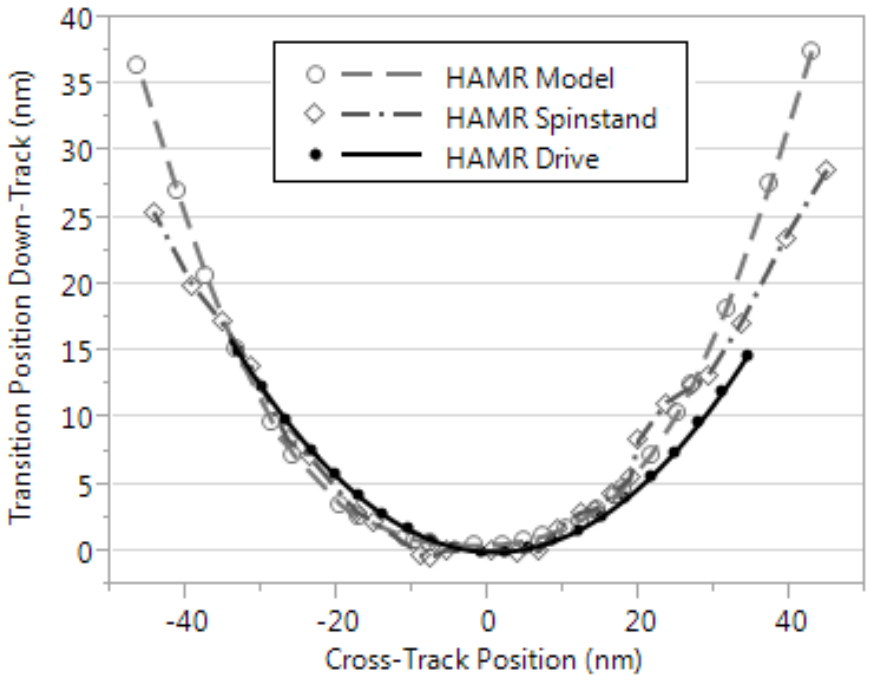

Figure 3.7: Comparison of modeled, spinstand, and HDD curvature results

The modeled and spinstand results assume a fixed track width of approximately 90 nm to determine the edges of the track, significantly larger than the track width at 50% amplitude of 68.5 nm measured in drive, making it difficult to compare the maximum down-track offset. However, if we truncate the modeled and spinstand profiles to assume the same track width as our drive measurement, we can use corrected down-track offsets of 24.116 nm and 18.169 nm for the modeled and spinstand respectively.

Upon visual inspection, all three methods appear very similar in the region near the track center, however the comparison that is of most interest in the context of this section is between the drive and spinstand measurements since both results were found experimentally. The agreement between the LLG model and spinstand has already been discussed in the study that produced the data[4]. The discrepancy between drive and spinstand measurements in this example is considerably less than one standard deviation for both curvature metrics, and therefore as a rule of thumb[33] we can conclude that the agreement between them is satisfactory. In more explicit terms, the difference between the experimental methods is too small to reject the null hypothesis that both results are equal with any statistical significance.

Chapter 4 – Experimental Study of HAMR Curvature

4.1 Comparison to Perpendicular Recording

Consistent with the ADC comparison provided in section 2.3, conventional (non-shingled) perpendicular recording is used as the reference case for transition curvature analysis. Experimental spinstand studies[4,8] have shown that HAMR transitions have significantly more curvature than PMR, which is thought to impose a substantial limitation on linear density in HAMR[26]. In figure 4.1, we demonstrate that the increased curvature with HAMR is observed in HDD testing.

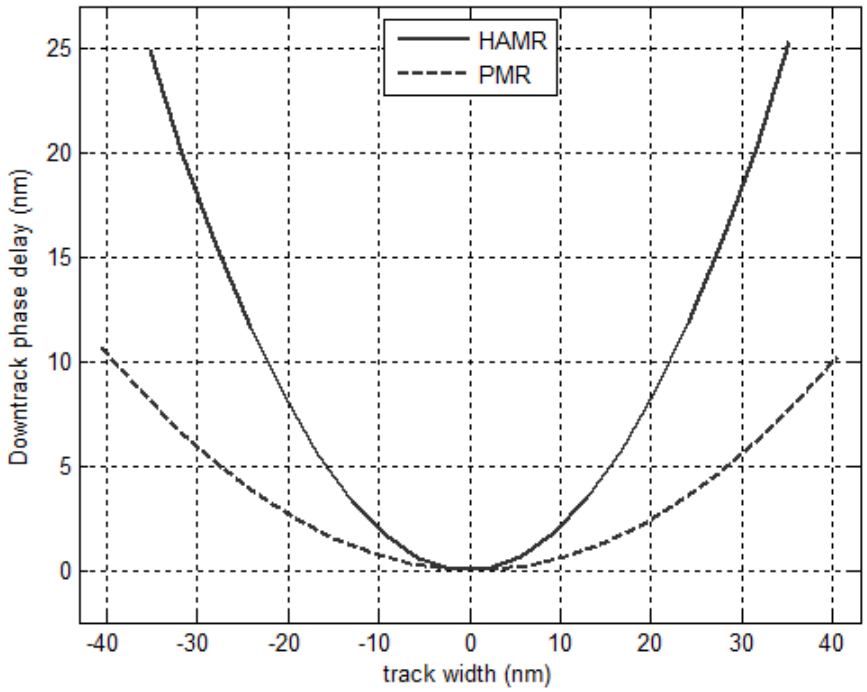

Figure 4.1: HDD curvature profile comparison between HAMR and PMR

The comparison provided in figure 4.1 shows an average HAMR curvature profile with curvature metrics that are 2-3 times greater than the accompanying PMR profile. The HAMR profile has a curvature coefficient value of 0.021 nm^{-1} and maximum down-track shift of 25.3 nm compared to an average PMR curvature profile with a coefficient of 0.0063 nm^{-1} and a maximum down-track shift of 10.7 nm.

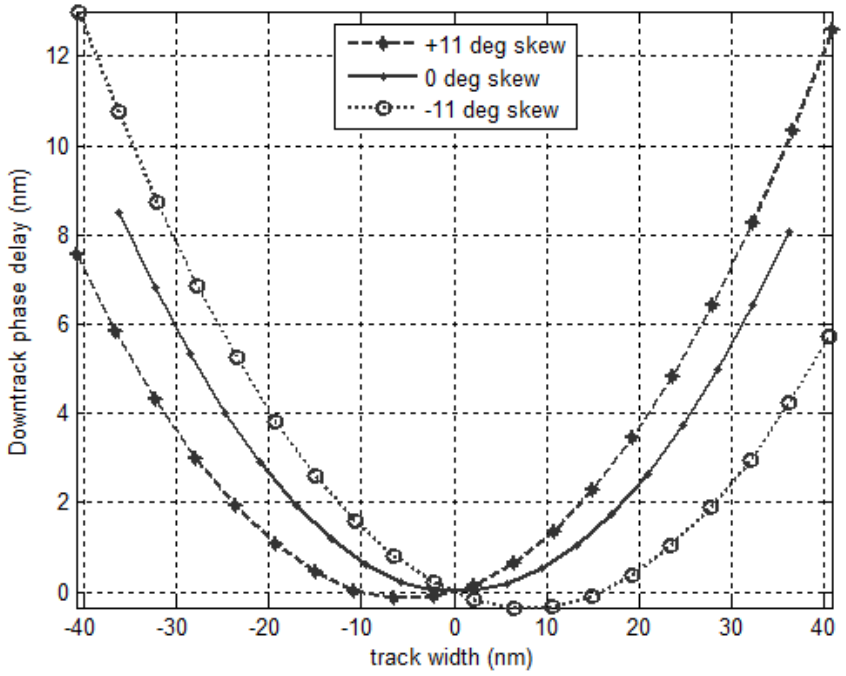

Figure 4.2: PMR curvature profiles measured at OD/MD/ID skew angles

Several experimental and theoretical studies[18,21] have been published on characterizing transition curvature in PMR and the impact it has on areal density. The curvature in PMR transitions is primarily attributed to contours of the switching field distribution in the media during the write process[25]. It has been demonstrated that modifying the geometry of the trailing edge of the main write

pole has a significant influence on the shape of the transition[23]. It has also been shown that through the same mechanism, changing the skew angle can introduce asymmetry into the recording characteristics[27]. This asymmetric effect is observed experimentally through drive testing by the three curvature profiles in figure 4.2 measured in a production PMR HDD at zero skew and +/- 11° skew angles. The OD, MD and ID profiles have respective curvature coefficients of 0.0057 nm^{-1}, 0.0064 nm^{-1}, and 0.0061 nm^{-1}, and maximum shifts in down-track position of 13.37 nm, 9.45nm, and 12.77 nm. This observed transformation in profile shape that is induced by changing skew angle is discussed at length in section 4.2.

4.2 Skew Angle

Throughout the catalog of published research on transition curvature in PMR, little effort has been devoted to the interaction between transition shape and skew angle. In this section, we examine how the transition curvature changes across the full stroke of the actuator, and find the sensitivity to be dominated by head skew. The influence of head skew on transition curvature in HAMR can be decomposed into two main effects: increased asymmetry of the profile shape, and a slight decrease in the coefficient of curvature.

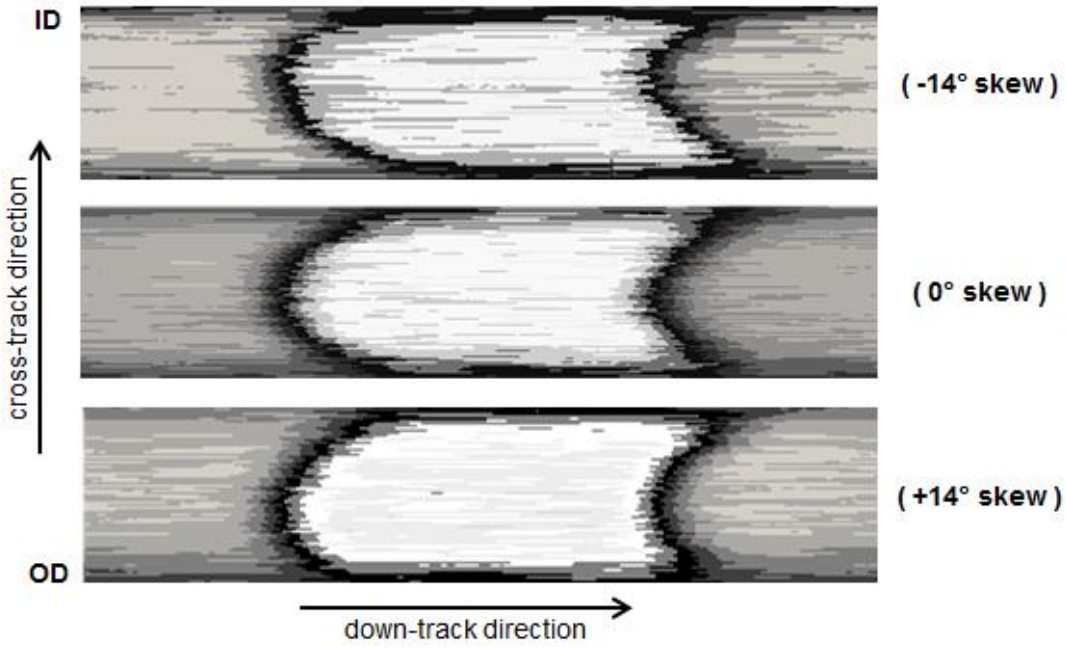

Figure 4.3: HAMR footprint images showing the impact of head skew

4.2.1 Curvature profile asymmetry

The transition curvature in a HAMR HDD becomes increasingly asymmetrical as the head moves away from zero skew. Footprint images and their corresponding curvature profiles measured at zero skew and at +/- 14° skew angles are provided in figures 4.3 and 4.4 respectively, resembling the behavior observed with PMR in figure 4.2. As the skew angle is increased, the "nose" of the profile shifts away from the center of the track by as much as 10 nm, moving radially away from zero skew. This causes a balanced shift in the down-track offsets where the transition meets the edges of the track, increasing by ~10 nm on the side closest to the MD and decreasing by a similar amount on the opposite side. The net result is a 10 nm increase in the maximum down-track

offset. The transformation of the curvature profile occurs with mirrored symmetry around the zero-skew radius, suggesting that head skew is the primary factor driving this change and that the contribution of linear velocity is negligible.

To better understand the curvature profile asymmetry, we examine how the geometry of the recording process changes with skew. Figure 4.5 provides a schematic drawing that illustrates the orientation of the write pole and media thermal spot when the head is positioned at zero skew compared to when a large skew angle is introduced by moving the head to the far ID of the disk. With the head positioned at the ID, the skew angle is reflected as a change in the angle between the leading edge of the write pole relative to track center.

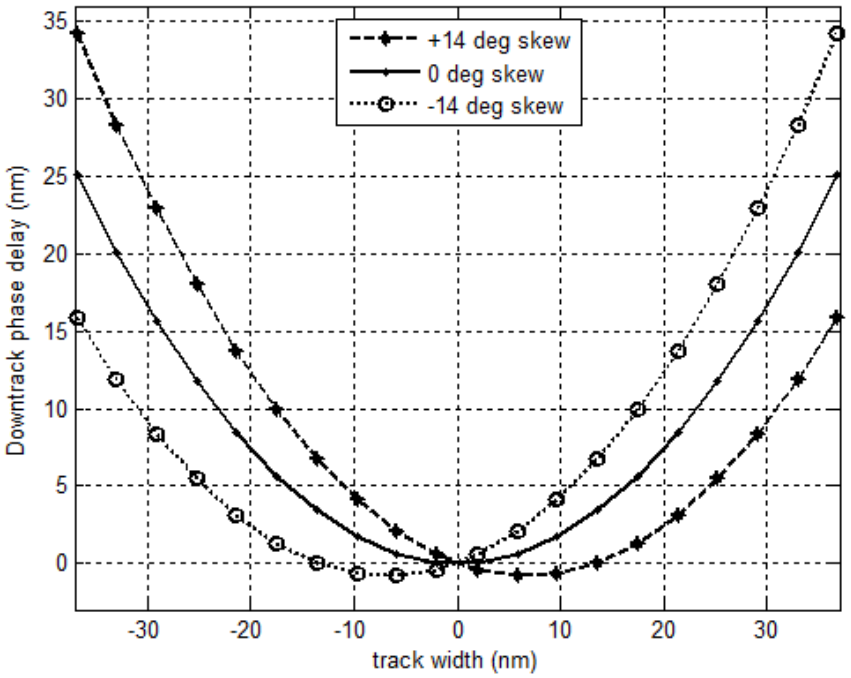

Figure 4.4: Fitted HAMR curvature profiles showing the impact of head skew

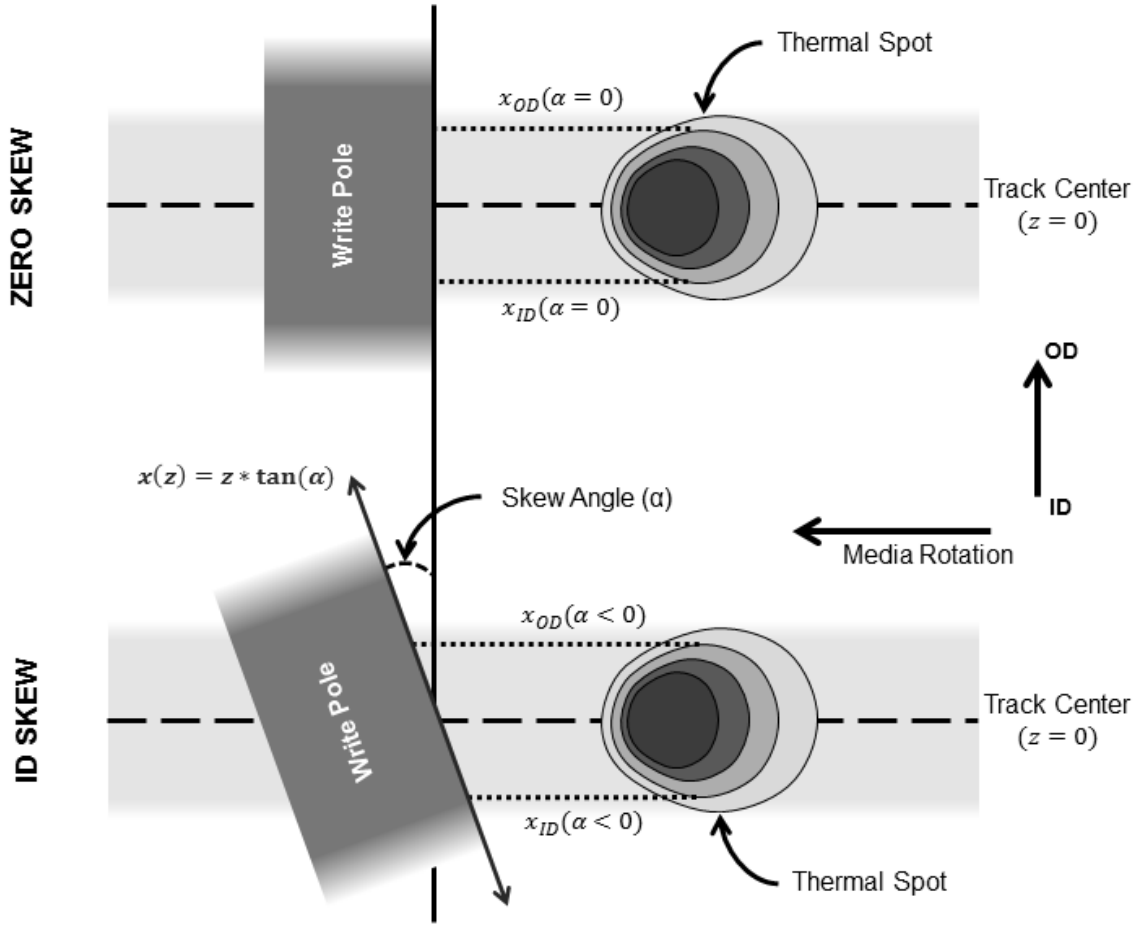

Figure 4.5: HAMR recording geometry change with skew angle

We define a set of axes along the cross-track and down-track directions with an origin at the point where the leading edge of the write pole intersects the center of the track. If we imagine a line that follows the leading edge of the write pole and extends infinitely in either direction, we can see that the slope of this line is determined by the tangent of the skew angle. The equation of this imaginary line (equation 4.1) establishes a reference for the location of the edge of the write pole in the down-track direction (x) as a function of cross-track

position (z) for a given skew angle (α). Taking the position of the write pole at zero skew (α = 0) as the nominal case, the change in the down-track location of the leading edge at a desired skew angle (α = α') is found by evaluating the expression x(z,α') – x(z,0), which simply reduces back to x(z,α').

$$x(z, \alpha) = z * \tan(\alpha) \tag{4.1}$$

We will assume for now that the influence of head skew on the shape and position of the thermal spot is negligible and also that the width of the write pole is much larger than the width of the thermal spot. Under these assumptions, applying equation 4.1 for a given skew angle directly reflects the change in down-track separation between the thermal spot and the write pole as a function of cross-track position. This skew-induced change in down-track spacing is depicted in figure 4.5 using dotted lines drawn between the write pole and thermal spot near the outer edges of the track. Examining the case where the head is positioned at an ID skew angle, the distance between the edge of the writer to the thermal spot has increased along the OD edge of the track ($x_{OD}(\alpha<0) > x_{OD}(\alpha=0)$), and similarly decreased along the ID edge of the track ($x_{ID}(\alpha<0) < x_{ID}(\alpha=0)$).

We understand intuitively that because the curvature profile is determined by fitting a quadratic polynomial to an independent variable (z), any asymmetry with respect to track center is represented entirely within the linear term of the resulting equation. Using this information, figure 4.6 reveals a nearly 1:1 correlation between the change in pole-to-spot spacing from equation 4.1 and the

curvature asymmetry as determined by the linear coefficient of the fitted quadratic equation. This data includes measurements from a sample of 8 HAMR HDDs that were each measured at 7 different skew angles across the media surface, showing the tangent of the skew angle on the horizontal axis and the first-order coefficient on the vertical axis.

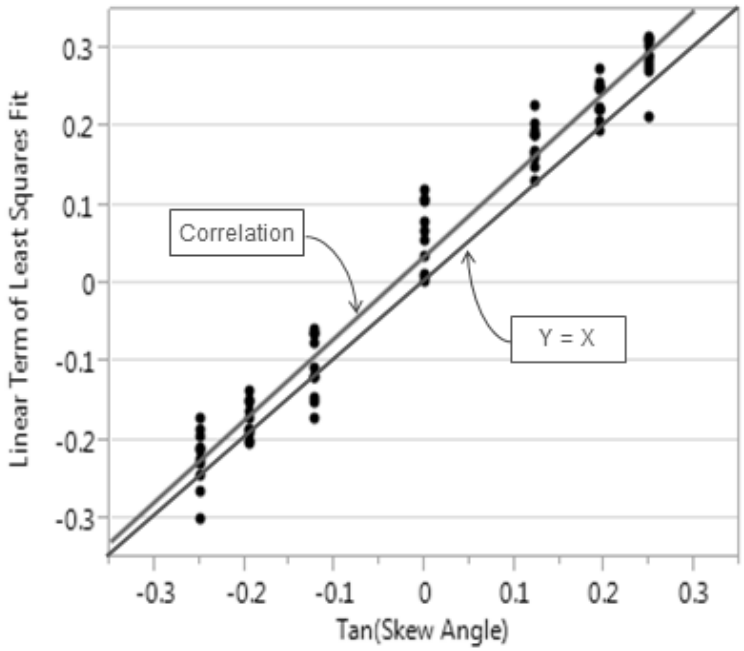

Figure 4.6: Predicted and measured curvature profile asymmetry

Knowledge of this relationship could provide a potentially useful way of estimating the shape of the profile at any skew angle if the curvature profile at a single location is known. Two such examples are given in figure 4.7 for curvature profiles at the OD and ID, with two curves being shown for each location. Solid lines are used to show the profiles that were fit to experimental data taken at their respective skew angles, and the dashed lines show very similar profiles that were

found simply by adding equation 4.1 to the equation of the curvature profile measured at zero skew.

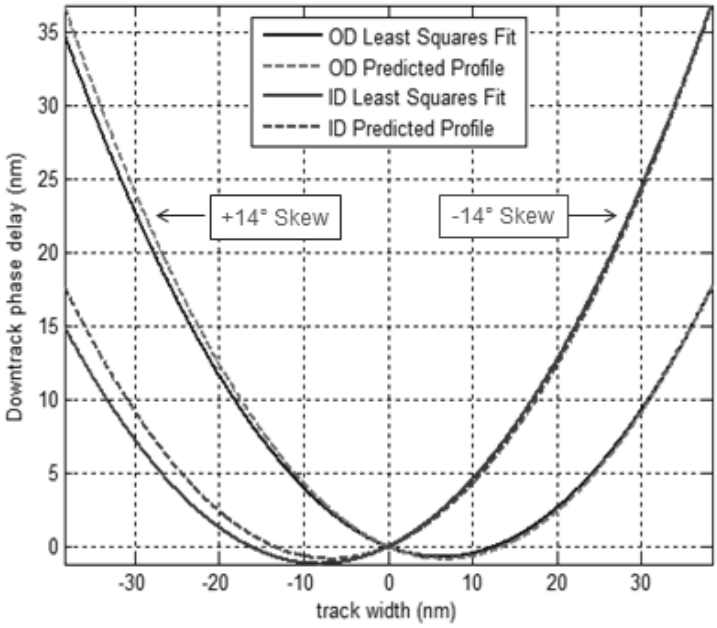

Figure 4.7: Comparison of actual vs predicted curvature profiles at OD and ID

A theoretical approach to correcting transition curvature in HAMR proposes the use of a write field with an amplitude that varies in the cross-track direction[26]. The principle behind this idea is to take advantage of the inverse relationship between applied field and the "freezing" temperature where recording occurs. The shape of the transition is determined by where the recording temperature occurs within the thermal profile. In the case of a uniform applied field, the recording temperature follows a single contour of the thermal gradient resulting in a transition that closely mimics the curved shape of the thermal profile. However, if an applied field profile that increases in strength with

its distance away from track center is used, recording will occur at a higher thermal contour at the track center and move to lower thermal contours towards the track edges. The end result is an effectively straightened transition shape, however this is achieved at the expense of a poorly defined transition in the low-field region.

The observation of skew-induced curvature asymmetry can be explained in a very similar manner. Given that our experimental data strongly supports a connection between curvature asymmetry and the orientation of the write pole, it seems reasonable to hypothesize that the underlying mechanism involves some amount of spatial variation in the effective write field within the vicinity of the thermal spot. We assume a write field that decreases in amplitude as the distance from the write pole increases. The decreasing field amplitude as a function of distance translates to an increasing recording temperature as a function of distance[26]. This implies that a change in distance from the write pole would cause the recording temperature to move to a different contour of the thermal profile. In the case of a head positioned at an ID skew angle shown in figure 4.5, the increase in spacing from the write pole at the OD side of the track would shift the recording temperature to a higher thermal contour that is closer to the peak of the thermal profile. Similarly, the recording temperature at the ID side of the track would shift to a lower thermal contour away from the profile peak. The end result is a recorded transition that has deviated asymmetrically from the true shape of the thermal spot.

4.2.2 Curvature coefficient sensitivity to skew

In addition to the dramatic differences in profile shape, a less obvious skew-related sensitivity is found in the actual amount of curvature. It is difficult to observe by just looking at the OD/MD/ID profiles due to the large amount of curvature and asymmetric profile distortion; however figure 4.8 shows the quadratic coefficient of 8 HAMR drives measured at seven different skew angles distributed across the stroke.

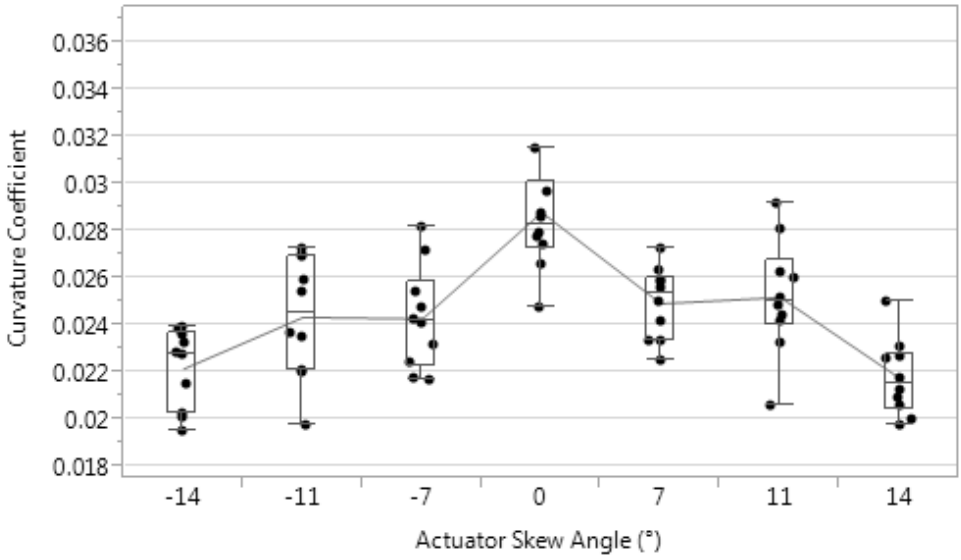

Figure 4.8: Curvature coefficient as a function of actuator skew angle

The curvature coefficient distributions show a peak in curvature coefficient at zero skew and a small yet statistically significant decrease in curvature as the head moves away from zero skew. It is worth pointing out that although a ~0.006 nm^{-1} difference may appear small compared to the total overall curvature of the transition; this delta alone would account for nearly the entire amount of

curvature in a PMR transition profile. Also, similar to the asymmetry effect discussed in the previous section, this coefficient reduction occurs symmetrically about the zero-skew radius, suggesting that linear velocity does not make any significant contributions to the curvature profile.

4.3 Laser Power

In the past we have shown that changing the power applied to the laser, and consequently the heat energy transferred into the media, has a direct influence on a number of variables in the drive, including on-track error rate, write sensitivity to head-to-media spacing, track width, ambient temperature, linear velocity, and ADC[6].

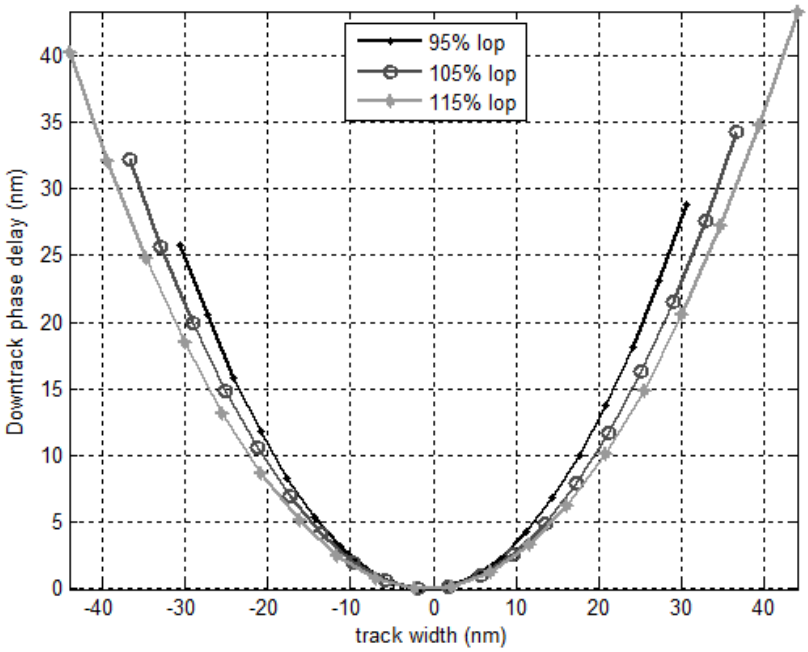

Figure 4.9: Curvature profiles measured at different applied laser powers

We can also show the effect that changing laser power has on transition curvature. Figure 4.9 shows the average curvature profile measured at zero skew at different laser power settings, normalized to the initially calibrated laser power and increasing in increments of 5% of the effective laser power. For clarity, the curvature profiles measured at 100% and 110% effective laser power settings are omitted from figure 4.9.

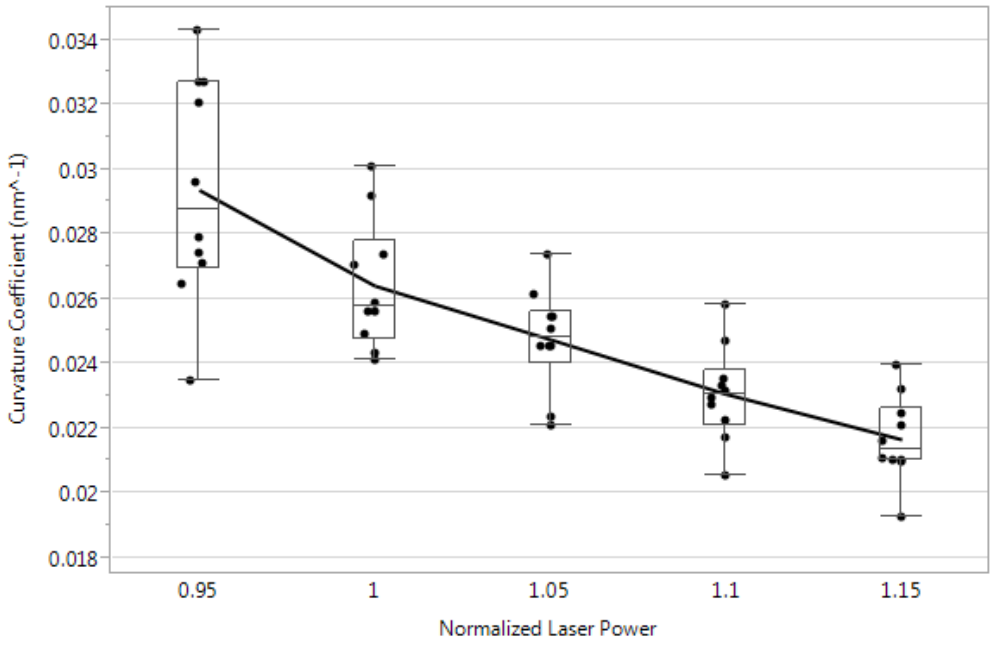

Figure 4.10: Transition curvature coefficient decreasing with laser power

Consistent with early modeled predictions[3] and recent experimental observations[5], we observe three effects occurring simultaneously as laser power increases: an increase in width of the track, an increase in the maximum down-track shift of the transition location, and a decrease in the curvature coefficient. It has been shown previously[6] that the width of the track increases linearly with

laser power above a certain point. In this case, the expansion occurs at ~1.4 nm per percent change in laser power. The reduction in transition curvature coefficient given in figure 4.10 also appears to follow a fairly linear trend with laser power, with a mean difference of 0.0077 nm^{-1} across the 20% range of laser power tested, with a statistical uncertainty of +/-0.0019 nm^{-1}.

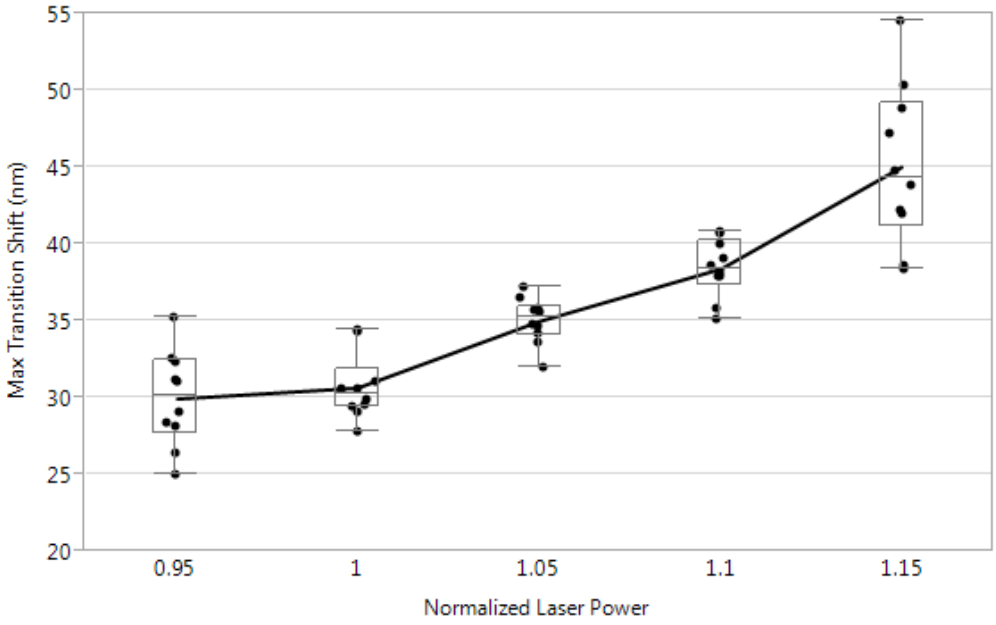

Figure 4.11: Maximum down-track phase shift sensitivity to laser power

The increase in maximum down-track transition position is 15.14 nm, with a statistical uncertainty of +/- 2.76 nm. Unlike the track width and curvature coefficient, a linearity of the dependence on laser power in figure 4.11 is not as easily apparent. All three of these effects can be attributed to a thermal profile that increases in amplitude with laser power due to more optical energy being

coupled into the media, which causes the diameter of the thermal contour where the temperature approaches T_c to also increase.

We can show in figure 4.12 that the reduction in curvature with laser power is consistent across the stroke. Qualitatively, the coefficient sensitivity to skew angle shown in section 4.2.2 appears to flatten out when laser power is increased, however the sample size in this case is too small to support this observation statistically.

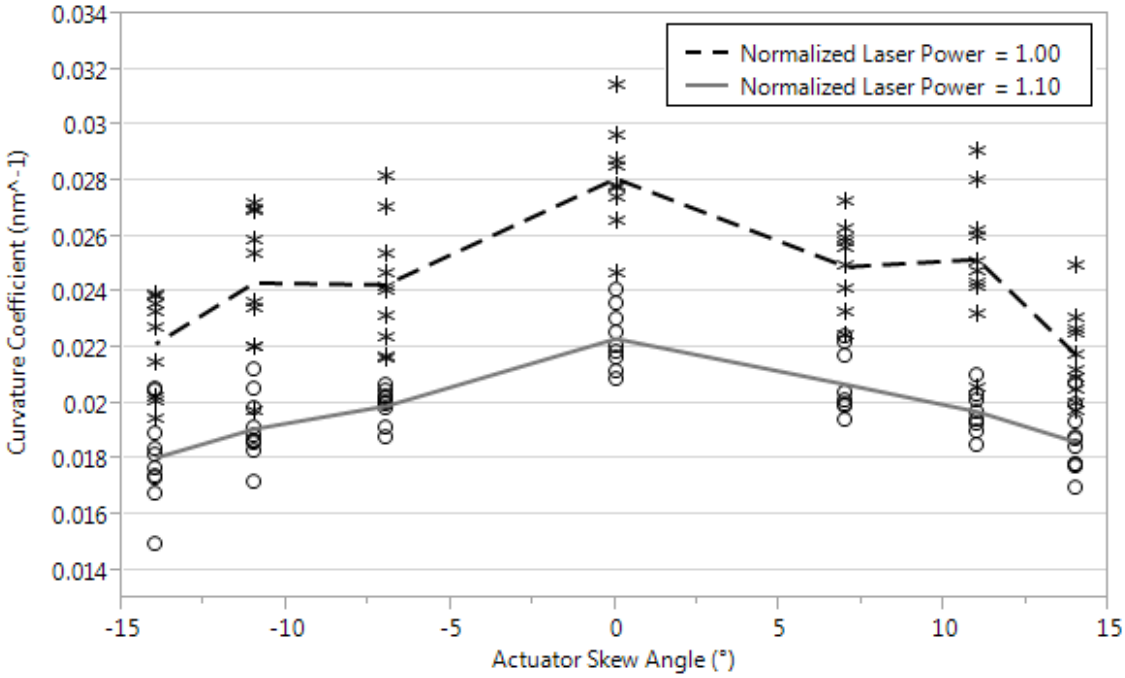

Figure 4.12: Laser power effect on curvature coefficient across the stroke

One final thought on laser power sensitivities is that because laser power is coupled with many environmental variables, an understanding of these effects is not only beneficial for improving recording performance, but also provides an easy sanity check to show that experimental results are not artifacts of other

uncontrolled variables. For example, referring back to the coefficient sensitivity to skew angle in figure 4.8, it would be reasonable to question if the observed change in curvature was actually the result of variation in calibrated laser power. Not shown in section 4.2.2 is the track width that was measured at each skew location, which does show some variation across the stroke on the order of a few nanometers. We now know that the curvature decreases by an average of 0.00039 nm^{-1} per percent change in laser power, explaining the 0.006 nm^{-1} curvature difference in figure 4.8 would require an ~15% variation in laser power. With the rate of track width expansion found to be ~1.4 nm per percent change in laser power, the resulting variation in measured track width would need to be ~22 nm. This amount of variation is an order of magnitude larger than what was actually observed, supporting the hypothesis that an actual geometric profile dependence was detected in our experiment. While the experimental results appear to be valid, more work is needed to understand the physical root cause of this effect.

Summary

The characteristics of areal density capability in a hard disk drive are impacted by the location where the data is recorded on the disk. The factors that contribute to this change in a HAMR drive are different from conventional PMR. The curvature of the written transition is one of the variables contributing to this difference. It has been demonstrated that the impact of finite reader width effects on magnetic footprinting can be sufficiently mitigated in HDD testing by using a transverse microtrack approach, and measurements of the curvature of a written transition can be performed with acceptable repeatability and are consistent with expectations based on prior modeling and spinstand work. It has been shown that transitions written with HAMR have much higher curvature than those written with PMR, and skew angle and applied laser power have been shown to significantly impact transition curvature. Both PMR and HAMR technologies exhibit a similar characteristic change in profile shape that depends on skew angle. For the case of HAMR, we have shown that this change has a high correlation to the geometry of the write pole as a function of skew angle, and discussed a possible explanation based on an interaction between changing distance between the write pole and thermal spot combined with spatial variation in the write field in the vicinity of the thermal spot. Increasing skew angle has also been shown to cause a decrease in the amount of curvature. As the applied laser power in a HAMR system is increased, the size of the thermal profile in the

media also increases, resulting in a simultaneous decrease in curvature and increase in track width and maximum down-track shift in transition location. The measured curvature and track width response to laser power has been shown to provide additional evidence to support observed curvature dependence across the stroke. While significant insight to the behavior of transition curvature in an HDD has been provided, the change in curvature across the stroke does not explain the radial dependence of ADC, and therefore more work is needed to fully understand this and other factors that limit areal density growth for HAMR.

Bibliography

1. H. N. Bertram, “Theory of Magnetic Recording”, Cambridge University Press, 1994, ISBN 0-521-44973-1
2. C. Mee, “Magnetic Recording Technology”, McGraw-Hill Professional, 2nd edition, 1996, ISBN-10: 0070412766
3. M. Kryder, *et. al.*, “Heat Assisted Magnetic Recording”, Proc. IEEE, vol. 96, no. 11, pp. 1810-1835, Nov. 2008
4. C. Rea, *et. al.*, “High Track Pitch Capability for HAMR Recording”, *IEEE Trans. Magn.*, vol. 53, no. 2, Feb. 2017
5. R. Eaton, A. Moser and D. Wolf, “Imaging of the Thermal Spot in Heat Assisted Magnetic Recording”, *IEEE TMRC 2016*, Paper A3
6. M. Cordle, *et. al.*, “Radius and Skew Effects in an HAMR Disk Drive”, *IEEE Trans. Magn.*, vol. 52, no. 2, Feb. 2016
7. S. Granz, *et. al.*, “Definition of an Areal Density Metric for Magnetic Recording Systems”, *IEEE Trans. Magn.*, vol. 53, no. 2, Feb. 2017
8. C. Rea, *et. al.*, “Areal-Density Limits for Heat-Assisted Magnetic Recording and Perpendicular Magnetic Recording”, *IEEE Trans. Magn.*, vol. 52, no. 7, July 2016

9. C. Y. Tseng, *et. al.*, “Transition Curvature and Transition Broadening Analysis Using the Spin-Stand Imaging Technique”, *IEEE Trans. Magn.*, vol. 47, no. 10, October 2011

10. D. J. Seagle, *et. al.*, “Transition Curvature Analysis”, *IEEE Trans. Magn.*, vol. 35, no. 2, March 1999

11. E. Grochowski and R.D. Halem, “Technological Impact of Magnetic Hard Disk Drives on Storage Systems”, *IBM Systems Journal*, 42(2):338-346, 2003

12. C. Ruemmler and J. Wilkes, “An Introduction to Disk Drive Modeling”, *IEEE Computer*, 27(3):17-29, March, 1994

13. A. Sagiroglu and D. Sinanc, “Big Data: A Review”, *International Conf. on Collaboration Technologies and Systems*, San Diego, CA, 2013, pp. 42-47

14. T. Rausch, *et al.*, “HAMR Drive Performance and Integration Challenges”, *Proc. IEEE*, vol. 49, no. 2, pp. 730-733, Feb. 2013

15. C. Vogler, *et al.*, “Efficiently reducing transition curvature in heat-assisted magnetic recording with state-of-the-art write heads”, *Cornell University Library*, arXiv:1703.00749, March 2017

16. J. Gantz and D. Reinsel, “The Digital Universe in 2020”, *IDC Go-to-Market Services Report*, Dec, 2012

17. B. M. Lairson, *et al.*, “Disk Drive Integration Issues for Perpendicular Recording”, *IEEE Trans. Magn.*, vol. 37, no. 4, July 2001

18. F. Liu, *et al.*, “Quantitative analysis of transition curvature by magnetic force microscopy”, *J. Appl. Phys.*, vol. 91, no. 10, May 2002

19. H. Zhou and R. Gustafson, “Effects of Head Pole Aspect Ratio and Skew Angle on Areal Density in Perpendicular Recording”, *IEEE Trans. Magn.*, vol. 40, no. 4, July 2004

20. I. D. Mayergoyz, *et al.*, “Magnetic imaging on a spin-stand”, *J. Appl. Phys.*, vol. 87, no. 9, May 2000

21. M. Hashimoto, *et al.*, “Analysis of Written Transition Curvature in Perpendicular Magnetic Recording From Spin-Stand Testing”, *IEEE Trans. Magn.*, vol. 43, no. 7, July 2007

22. P. A. A. van der Heijden, *et al.*, “Effects of transition curvature on perpendicular magnetic recording performance”, *Appl. Phys. Lett.*, vol. 83, no. 21, Nov. 2003

23. W.-C. Lin, *et al.*, “Precise Measurement of the Transition Curvature in Magnetic Recording”, *IEEE Trans. Magn.*, vol. 47, no. 10, Oct. 2011

24. Y. Jiao, Y. Wang and R. Victora, “A Study of SNR and BER in Heat-Assisted Magnetic Recording”, *IEEE Trans. Magn.*, vol. 51, no. 11, Nov. 2015

25. X. Che and N.-Y. Kim, “Transition Curvature Assessment for High TPI Applications”, *IEEE Trans. Magn.*, vol. 42, no. 10, Oct. 2006

26. J.-G. Zhu and H. Li, “Correcting Transition Curvature in Heat Assisted Magnetic Recording”, *IEEE Trans. Magn.*, vol. 53, no. 2, Feb. 2017

27. X. Chen *et al.*, “A Physical Model for Predicting Off-Track Capability in Perpendicular Recording”, *IEEE Trans. Magn.*, vol. 52, no. 9, Feb. 2016

28. D. Reinsel, J. Gantz and J. Rydning, “Data Age 2025: The Evolution of Data to Life-Critical”, *IDC white paper*, March 2017

29. L. Huang, et al., “HAMR Thermal Modeling Including Media Hot Spot”, *IEEE Trans. Magn.*, vol. 49, no. 6, June 2013

30. D. Weller and A. Moser, “Thermal Effect Limits in Ultrahigh-Density Magnetic Recording”, *IEEE Trans. Magn.*, vol. 35, no. 6, Nov. 1999

31. D. Saunders, *et al.*, “HAMR Thermal Gradient Measurements and Analysis”, *IEEE Trans. Magn.*, vol. 53, no. 2, Feb. 2017

32. P. McAvoy, *et al.*, “Spin-Stand Imaging of Perpendicularly Recorded Data”, *IEEE Trans. Magn.*, vol. 44, no. 11, Nov. 2008

33. J. R. Taylor, “An Introduction to Error Analysis”, 2nd ed., 1997, ISBN 0-935702-42-3

34. S. N. Piramanayagam, “Perpendicular recording media for hard disk drives”, *J. Appl. Phys.*, 102, 011301 (2007)

35. T. C. Arnoldussen and L. L. Nunnelley, “Noise in Digital Magnetic Recording”, *World Scientific Publishing Co. Pte. Ltd.*, 1992, ISBN: 981-02-0865-0

36. T. W. McDaniel, W. A. Challener, and K. Sendur, “Issues in Heat-Assisted Perpendicular Recording”, *IEEE Trans. Magn.*, vol. 39, no. 4, pp. 1972-1979, July 2003

37. American Society of Mechanical Engineers, “The IBM 350 RAMAC Disk File System”, Technical Brochure, Feb. 1984